ADVANCED FUNCTIONAL MATERIALS



DOI: 10.1002/adfm.200800447

# Growth, Cathodoluminescence and Field Emission of ZnS Tetrapod Tree-like Heterostructures**

By *Zhi-Gang Chen, Jin Zou, Gang Liu, Xiangdong Yao, Feng Li, Xiao-Li Yuan, Takashi Sekiguchi, Gao Qing Lu,** and *Hui-Ming Cheng**

We report the growth mechanism, cathodoluminescence and field emission of dual phase ZnS tetrapod tree-like heterostructures. This novel heterostructures consist of two phases: zinc blende for the trunk and hexagonal wurtzite for the branch. Direct evidence is presented for the polarity induced growth of tetrapod ZnS trees through high-resolution electron microscopy study, demonstrating that Zn-terminated ZnS (111)/(0001) polar surface is chemically active and S-terminated $(\bar{1}\bar{1}\bar{1})/(000\bar{1})$ polar surface is inert in the growth of tetrapod ZnS trees. Two strong UV emissions centered at 3.68 and 3.83 eV have been observed at room temperature, which are attributed to the bandgap emissions from the zinc blende trunk and hexagonal wurtzite branch, indicating that such structures can be used as unique electromechanical and optoelectronic components in potential light sources, laser and light emitting display devices. In addition, the low turn-on field ($2.66\,V\mu m^{-1}$), high field-enhancement factor (over 2600), large current density (over $30\,mAcm^{-2}$ at a macroscopic field of $4.33\,V\mu m^{-1}$) and small fluctuation (~1%) further indicate the availability of ZnS tetrapod tree-like heterostructures for field emission panel display. This excellent field-emission property is attributed to the specific crystallographic feature with high crystallinity and cone-shape patterned branch with nanometer-sized tips. Such a structure may optimize the FE properties and make a promising field emitter.

## 1. Introduction

Rational design and fabrication of nanostructures as building blocks for functional materials and devices are the key to tailoring properties for specific applications in electronics, optics, biomedicine, field emitter and micro/nanosystems.[1] Ionic crystals typically consist of alternating layers of positively charged cations or negatively charged anions, which have characteristically polarized surfaces, resulting in dipole moments and spontaneous polarization along some particular directions.[2] These dipole moments and divergence in surface energies may be compensated by creating new facets and/or massive surface reconstruction, which can significantly contribute to the asymmetric growth of unique nanostructures,[3] such as nanoribbons,[4,5] nanosprings,[6] nanorings,[7] nanohelices,[8] nanobows,[9] and nanotrees.[10] The driving force for the formation of these unique morphologies is the minimization of the electrostatic interaction energy of the polar surface.[2] To date, different compositive tetrapod nanostructures[11–18] were reported, however, to obtain patterned or ordered growth of tetrapods remains a great challenge. Here, we show that surface polarity can induce novel asymmetric growth of ZnS dual-phase tetrapod tree-like heterostructures (a single compound with two crystal phases). Two strong UV emissions centered at 3.68 and 3.83 eV have been observed from this unique heterostructure at room temperature, which are attributed to the bandgap emissions from the zinc blende for the trunk and hexagonal wurtzite for the branch. This novel structure also possesses superior field emission (FE) properties of low turn-on field of $2.66\,V\,\mu m^{-1}$, high field-enhancement factor (over 2600), large current density (over $30\,mA\,cm^{-2}$ at a macroscopic field of $4.33\,V\,\mu m^{-1}$) and lower fluctuation of FE current as small as ~ 1%. Although the work function of ZnS (7.0 eV) is larger than that of AlN (3.7 eV), SiC (4.0 eV), GaN (6 eV), Si (3.6 eV), carbon nanotubes (5 eV), $TiO_2$ (4.5 eV), and ZnO (5.3 eV), the FE properties of ZnS tetrapod tree-like heterostructures are comparable or even better than those materials because of their characteristic patterned branch with sharp tips. Therefore, ZnS tetrapod tree-like heterostructures

[*] Prof. H.-M. Cheng, Dr. Z.-G. Chen, G. Liu, Dr. F. Li
Shenyang National Laboratory for Materials Science
Institute of Metal Research, Chinese Academy of Sciences
Shenyang, 110016 (PR China)
E-mail: cheng@imr.ac.cn
Prof. G. Q. (Max) Lu, Dr. Z.-G. Chen, Dr. X.-D. Yao
ARC Centre of Excellence for Functional Nanomaterials School of Engineering and AIBN, The University of Queensland
Brisbane, QLD 4072 (Australia)
E-mail: maxlu@uq.edu.au
Prof. J. Zou
School of Engineering and Centre for Microscopy and Microanalysis
The University of Queensland
Brisbane, QLD 4072 (Australia)
Dr. X.-L. Yuan, Dr. T. Sekiguchi
Advanced Electronic Materials Center, National Institute for Materials Science
1-1 Namiki, Tsukuba, Ibaraki, 305-0444 (Japan)

[**] This work was supported by the Key Research Program of MOST, China (2006CB932703) and the Australian Research Council. We sincerely thank Prof. Enge Wang at Institute of Physics, Chinese Academy of Sciences, for very useful discussions in this work.

may be expected to be used in novel electric and optoelectronic devices such as field emitters, atomic force microscope (AFM) probes, etc.

ZnS generally possesses two crystal structures: hexagonal wurtzite (WZ) ZnS ($a = 0.3820$ nm and $c = 0.6260$ nm; JPCDS card: 79-2204) and cubic zinc blende (ZB) ZnS ($a = 0.5407$ nm; JCPDS card: 77-2100). Their closely-packed atomic plane is {111} plane for the ZB structure and {0001} plane for the WZ structure, which are the most common polar surfaces.[8] Therefore, for the ZB structured ZnS, the oppositely charged ions produce positively charged $\{111\}_{Zn}$ and negatively charged $\{111\}_{S}$ atomic planes; while for the WZ structured ZnS, the oppositely charged ions produce positively charged $(0001)_{Zn}$ and negatively charged $(000\bar{1})_{S}$ atomic planes. The Zn- and S-terminated surfaces exhibit very different chemical activities. Since the growth configuration of a nanostructure is governed by surface energy and growth kinetics, novel nanostructures may be induced.[5,19] In this paper, we report that the surface polarization and the surface termination are critical factors for governing the growth of ZnS dual-phase tetrapod heterostructures, which show extraordinary cathodoluminescent (CL) properties and superior FE properties.

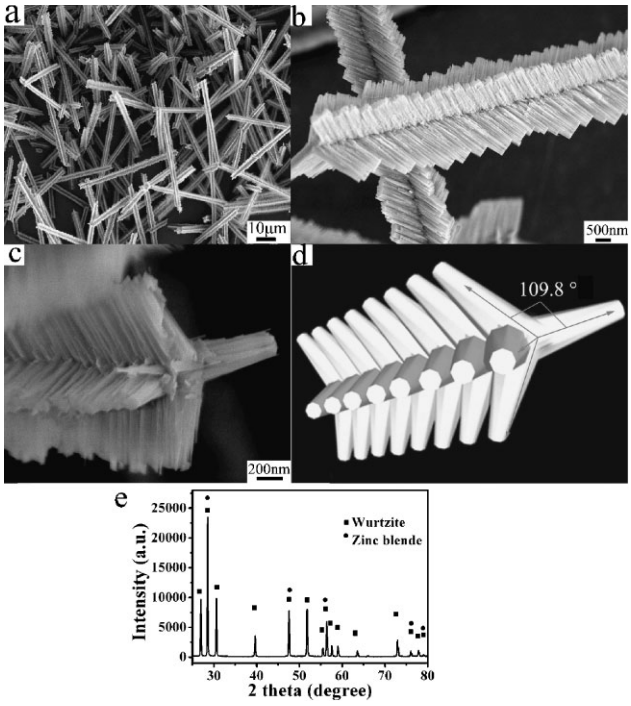


**Figure 1.** a)–c) SEM images showing general and detailed structural characteristics of the synthesized product. d) Structural model. e) XRD pattern showing two ZnS phases: WZ and ZB.

## 2. Results and Discussions

### 2.1. Characterization

The as-prepared sample was analyzed by scanning electron microscopy (SEM) demonstrating high purity, high yield, and structural control (Fig. 1a–d). Figure 1a shows general morphology of the synthesized product (their length is ca. tens of μm). Figure 1b shows the detailed structural characteristics of the synthesized product – tree-like branched structure with 4 uniform and parallel branches strictly with an equal length of 2 to 5 μm. Figure 1c and d display the orientational relationship of branches and their corresponding structural model. Figure 1e is a typical X-ray diffraction (XRD) pattern of these tree-like structures. All diffraction peaks can be exclusively indexed by WZ structure and ZB structure, suggesting that the synthesized product has a high purity, which agrees well with the SEM observations (such as Fig. 1a). Such patterns are similar to the reported XRD patterns of tetrapod ZnS[16] which the branches have the wurtzite phase and the core has the zinc blende phase. So, the novel tree-like branched structure can be considered as self-assembled tetrapod ZnS tree patterned by numerous ZnS tetrapods.

To understand the detailed structural characteristics of the synthesized product, transmission electron microscopy (TEM) investigations were carried out. Figure 2a and b show a pair of TEM images of a tetrapod ZnS, viewed in different directions with tilting along their axial direction for ca. 45 °. In Figure 2a, hierarchical four branched arrays with an equal length of ca. 2 μm can be seen protruding from the center (a wire-like trunk) to form a tetrapod structure; the V-shape branches of the tetrapod structure are clearly shown in Figure 2b, while the other two branched arrays are vertically aligned with the electron beam. Figure 2c is the selected area electron diffraction (SAED) pattern taken from the V-shape branches in Figure 2b and c shows a large number of diffraction spots. Careful analysis of these diffraction spots suggests that there exist two sets of diffraction patterns belonging to two $\pm[2\bar{1}\bar{1}0]$ WZ structures, as marked in Figure 2c. One thing may be noted that there are no spots belonging to ZB ZnS, because the electron beam couldn't penetrate another V-shaped WZ ZnS branches and ZB ZnS trunk when the V-shaped WZ ZnS branches are at the zone axis of $[2\bar{1}\bar{1}0]$. To determine the polarity of the branches, convergent beam electron diffraction (CBED) was used.[2] As shown in Figure 2d and e, the growth direction of branches can be uniquely determined to be [0001] for all cases. Figure 2f is a high-resolution TEM (HRTEM) image taken from the tip of a branch, which further confirms the branches having a WZ structure from the measured lattices with $a = 3.820$ Å and $c = 6.260$ Å. Figure 2g is a HRTEM image showing the interface between a trunk and a branch of the tetrapod heterostructure, which confirms that the trunk has ZB structure.

To elucidate the formation mechanism of these novel tetrapod heterostructures, the intermediate products were carefully characterized using both SEM and TEM. Figure 3a–c are a set of SEM images showing the morphology of a typical intermediate product (synthesized by 15 min under the identical synthesis conditions) viewed along different directions (tilted along the axial direction with relative titling angles of −30 °, 0 ° and 30 °). Figure 3d–f are high-magnification SEM

ADVANCED FUNCTIONAL MATERIALS



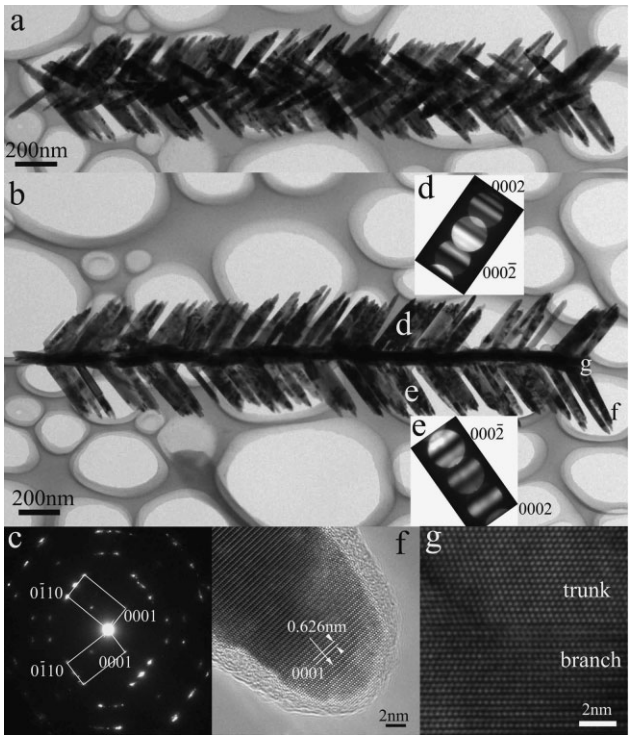


**Figure 2.** a) and b) A pair of TEM images showing a typical tetrapod structure viewed in different directions. c) The corresponding SAED pattern taken from a section in (b) showing two sets of diffraction patterns. d) and e) CBED patterns confirming the [0001] direction of branch. f) HRTEM image showing a branch of the tetrapod structure having the WZ structure. g) HRTEM image showing a trunk/branch interface with ZB/WZ structures.

images showing detailed surface morphologies of the intermediate product. As can be seen from Figure 3, the intermediate products have a wire-like structure with a squared cross-section. Interestingly, their sidewalls contain a number of nuclei. Branches initiating from these nuclei and inclining with the trunk can be found (marked in Fig. 3d–f).

Figure 4a and b are typical ⟨110⟩ on-zone TEM images of the intermediate products confirmed by their corresponding SAED patterns, which show that the trunks have ZB structure. Combining Figure 3 with Figure 4a and c, the axial direction of the intermediate product can be determined to be along ⟨100⟩ with the sidewalls lying on the {110} atomic planes. In Figure 4a, several faceted concave regions can be revealed and the facets are determined to be {111} planes, possibly due to its low surface energy for the f.c.c. lattice.[20] In Figure 4b, a large number of nuclei can be clearly seen on the sidewalls. The comparison of these nuclei, which initiate branches, with well developed branches (refer to Fig. 2b) suggests that branches are along the ⟨111⟩ directions of the ZB structured trunks. According to crystallography, the ZB structure possesses polarity, leading to $[u,v,w] \neq [\overline{u},\overline{v},\overline{w}]$ and $(h,k,l) \neq (\overline{h},\overline{k},\overline{l})$. Since the 8 possible ⟨111⟩ directions in a ZB structure belong to two equivalent groups (each contains 4 equivalent directions that can be denoted as $\langle 111\rangle_A$ and $\langle 111\rangle_B$), the fact that branches are developed into 4 ⟨111⟩ directions and formed tetrapod heterostructures suggests that the branches must be initiated by polarity. To determine the polarity of trunks, CBED was used.[21] Figure 4c and d are a pair of CBED patterns; from which, the dark and bright crosses can be determined as $(\bar{2}00)^*$ and $(200)^*$, assuming the zone axis being

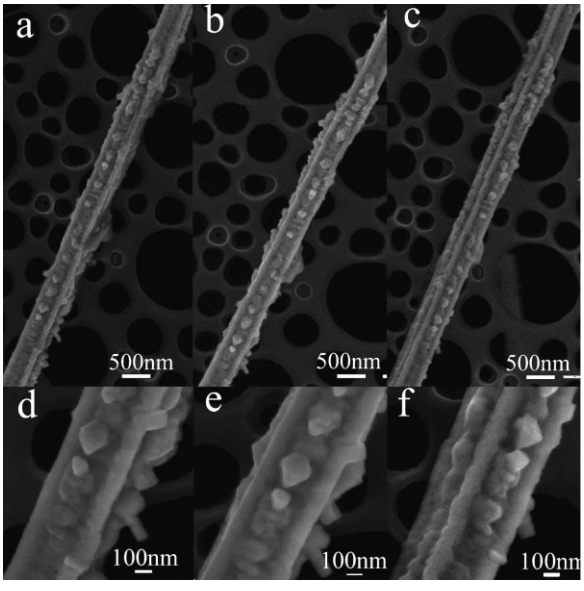


**Figure 3.** a)–c) Typical SEM images of a typical intermediate ZnS product (tilted along the trunk with angles of +30°, 0°, –30°. d) and e) Their corresponding high-magnification SEM images.

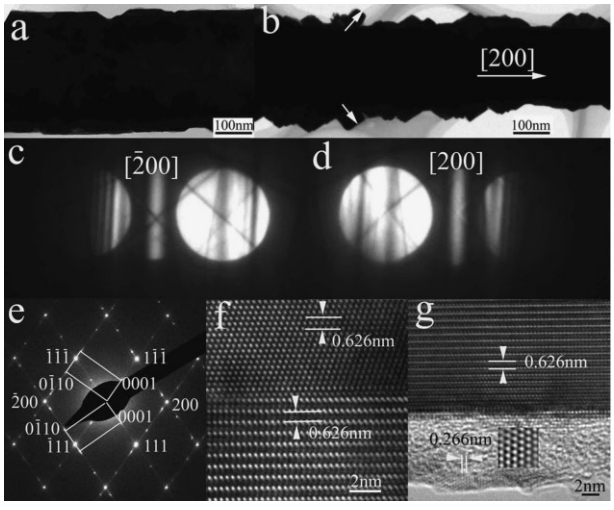


**Figure 4.** a) and b) ⟨110⟩ on-zone bright-field TEM images: a) Showing wire-like core with {111} faceted concave regions and b) Showing initiated branches along ⟨111⟩ direction. c) and d) Confirming CBED patterns which is the $(\bar{2}00)^*$ and $(200)^*$ diffractions, where the crosses were indexed respectively by $\{955\}^*$ and $\{\bar{7}55\}^*$. e) SAED pattern of (b) showing three sets of diffraction patterns – the $[01\bar{1}]$ zone axis of a ZB structure superimposed with the $\pm[2\bar{1}\bar{1}0]$ of two WZ structures. f) HRTEM image of a branch-trunk interface showing the branch having the WZ structure and the trunk having the ZB structure. g) HRTEM image of a branch's growth front, confirming the existence of Zn nanoparticles.

[$01\bar{1}$] (this assumption is used for the convenience of the discussion and does not influence the conclusion). Figure 4e is a SAED pattern taken from Figure 4b and shows the coexistence of the WZ and ZB structures with some orientation relations between the two phases: $\pm[2\bar{1}\,\bar{1}0]//[01\bar{1}]$ (the directions parallel to the electron beam) and {0001}//{111}. From the polarity determined in Figure 4c and d, the two $\{111\}^*$ diffraction spots close to $(200)^*$ can be determined to be $(111)^*$ and $(1\bar{1}\bar{1})^*$ (they all belong to $\{111\}_A$). Since the directions of the initiated branches (typically marked in Fig. 4b) are parallel to these two directions, we anticipate that the branches are initiated from $\{111\}_A$, i.e., $\{111\}_{Zn}$, of the trunk. Figure 4f is a HRTEM image taken from the interface between a newly-initiated branch and the underlying trunk, showing clearly the structural change from the ZB structured trunk to the WZ structured branch.[22] Figure 4g shows a $[2\bar{1}\,\bar{1}0]$ HRTEM image recorded from the growth front of an initial branch. It is of interest to note that the front surfaces are rough, and there are tiny nanocrytals being formed at the growth front. The processed (using Fast Fourier transformation) HRTEM image (refer to the inset) indicates that these nanoparticles are hexagonal Zn phase[23] with the lattice parameter of $a = 2.665$ Å and $c = 4.947$ Å (JCPDS card: 87-0713). Such extraordinary features demonstrate that the two phase growth characteristic observed from the ZnS tetrapod structures with crystallographic asymmetric structures apparently results from the different growth rates on positively charged (0001)/(111)-Zn and negatively charged $(000\bar{1})(\bar{1}\,\bar{1}\,\bar{1})$-S surfaces.

### 2.2. Growth Mechanism

Based on these results, the formation of tetrapod heterostructures is considered to occur in a two-step process, as illustrated in Figure 5: (1) the formation of the ZB structured ZnS trunks that have ⟨100⟩ axial directions with squared cross-section and {110} sidewalls; and (2) the formation of the WZ structured branches along the [0001] directions. To understand the formation of the ZB structured ZnS trunks, we repeated the experiment with a lower deposition temperature (ca. 680 °C). The ZB structured ZnS trunks with squared sidewalls and without branches were obtained. It has been reported that, for ZnS, the energy per atom for the ZB structure is slightly lower than that for the WZ structure, indicating that the ZB structure is relatively more stable than that of the WZ structure.[24] Therefore, the formation of the ZB structured ZnS trunk must be governed by thermodynamics. It has been well documented that the growth direction of cubic structured wires is along ⟨100⟩ with sidewalls of {110} due to their relatively low surface energies.[25,26] To understand the driving force for the branch formation and why the branches have a WZ structure, we should examine the surface structure of ZB and WZ phases in one-dimensional (1D) nanostructures. The branch grows in the favorite growth direction along the *c* axis (0001) with exposed surface being $\{01\bar{1}0\}$. The *c* axis of WZ corresponds to the ⟨111⟩ direction of ZB. If [111] is the growth direction for the ZB branch, the exposed surfaces would be {110} or {211}. In fact, the branch growth along the [0001] direction with exposed $\{01\bar{1}0\}$ side surfaces is likely to have the lowest surface energy.[22] This surface energy-driven phase transformation is further enhanced with the increased surface-to-volume ratio. After the nucleation, the growth of the branch along the stacking direction of closely-packed plane will prefer ABAB instead of ABCABC sequence to expose the $\{01\bar{1}0\}$ side surfaces. As a conclusion, the comparable low surface energy of $\{01\bar{1}0\}$ plane takes the key role in stabilizing the wurtzite phase in branch nanostructures. This is the reason that the branches of dual phase tetrapod heterostructure are WZ rather than ZB. Moreover, we note that, as shown in Figure 4g, the (0001)-Zn surface tends to have tiny Zn clusters at the growth front of branches. The Zn clusters as well as the local enrichments in Zn at the growth front tend to initiate the growth of ZnS similar to the vapor–liquid–solid (VLS) growth process. Therefore, the self-catalyzed effect of the Zn clusters results in a fast growth of branches. On the contrary, the $(000\bar{1})$-S terminated surface is likely to be inert and may not exhibit an effective self-catalyzed effect; thus, the surface may not initiate the growth of branches. Since the Zn planes are fast growth planes and the difference between the energy per atom for both the ZB and WZ structures are marginal,[24] we believe that the Zn induced fast growth of branches can easily lead to the formation of the WZ structure, where the branch growth along the [0001] direction with exposed $\{01\bar{1}0\}$ side surfaces is likely to have the lowest surface energy.

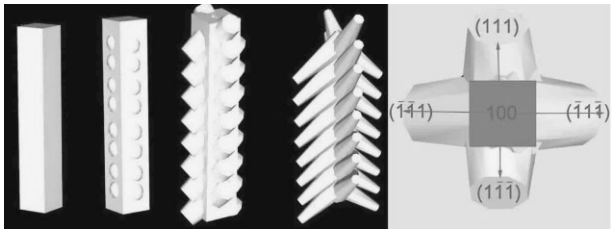


**Figure 5.** The schematic illustration of the formation of ZnS tetrapod tree-like heterostructures.

### 2.3. CL Properties

ZnS, as an important semiconductor compound of the II-VI group with the direct wide band gap (3.72 eV for the cubic ZB phase[27] and 3.77 eV for the hexagonal WZ phase[28] at the room temperature), is one of the first and most important semiconductors discovered and explored in the electronic and optoelectronic industry.[29] The optoelectronic properties of the nanostructures depend on their particular size, shape and local dielectric environment.[30] High-quality ZnS nanostructures having uniform shape and good optical properties at room temperature have rarely been reported. Therefore, we carefully analyzed the CL properties of the product. Figure 6 shows CL spectra at room temperature taken from the dual-phase tetrapod heterostructure and the similar diameter WZ and ZB phase ZnS nanowires. The spectrum of dual-phase tetrapod heterostructure shows two strong intrinsic emissions

ADVANCED FUNCTIONAL MATERIALS



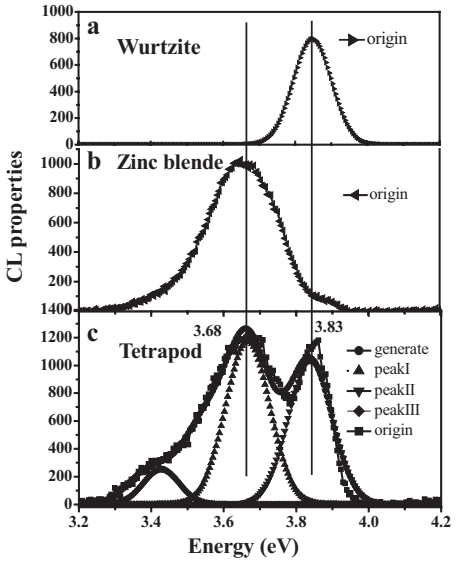


**Figure 6.** CL spectra of a single nanostructure. a) Dual-phase tetrapod heterostructure. b) ZB ZnS nanowire. c) WZ ZnS nanowire.

centered on 3.68 (peak I, 336 nm) and 3.83 eV (peak II, 323 nm) with a shoulder centered around 3.42 eV (peak III, 362 nm), as shown in Figure 6a. The peak I is typical CL emission from ZB bulk ZnS material, but slightly below the reported energy band gap of ZB ZnS epilayers (3.72 eV).[27] The peak I is also consistent with the experimental value (3.66 eV),[31] but far below the theoretical calculation value (3.98 eV).[32] The peak II has a slight blue-shift (to ca. 0.05 eV) compared to the reported 3.77 eV for the hexagonal WZ phase.[28,31] This implies that the tetrapod heterostructures display electron confinement or strain effects.[33] However, the Bohr diameter of bulk ZnS materials is ca. 5 nm,[34] such small blue-shift may be attributed to strain effect from the cone-shape WZ nanowires of the branch. To double-confirm the origination of each emission, we selected similar diameter nanowires for CL analysis, as shown in Figure 6b and c. Clearly, the peak I and peak II can be attributed to the band-energy emissions from ZB and WZ phase ZnS. The peak III is a new near-band emission. Compared with band-energy emission peak I and peak II, the peak III may be attributed from the native interface between the WZ and ZB phase of the dual phase tetrapod tree-like heterostructures.

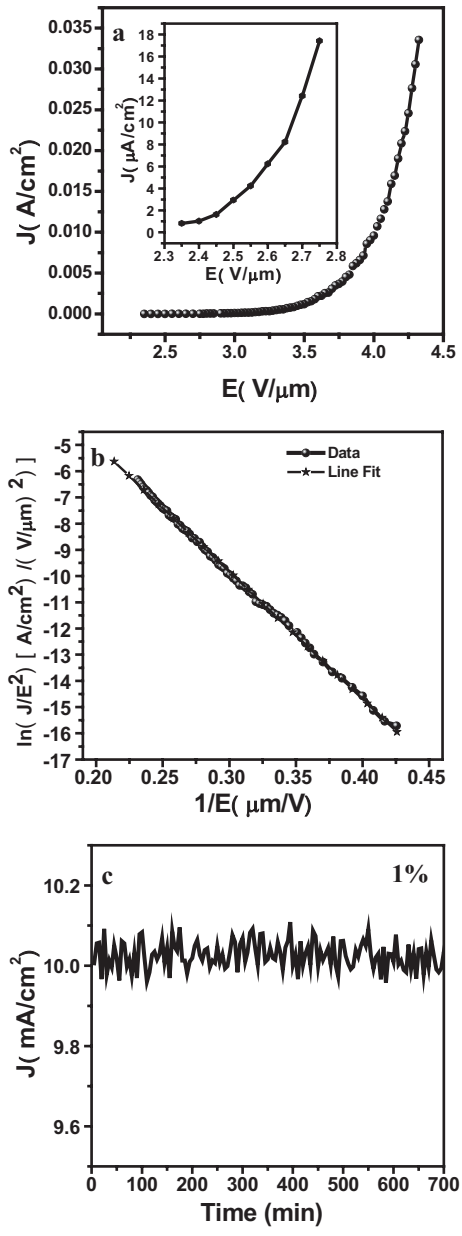


**Figure 7.** FE properties of ZnS tetrapod tree-like heterostructures: a) *J*–*E* plots of the sample. The inset is a magnified *J*–*E* curve with a turn-on field of ca.2.66 V $\mu m^{-1}$ at a current density of 10 $\mu A\ cm^{-2}$ b) A Fouler–Nordheim plot corresponding to (a), the straight line is a linear fit of the $\ln(J/E^2)$–$(1/E)$ plot. c) Field emission current stability of the ZnS heterostructures.

### 2.4. Field Emission

ZnS tetrapod tree-like heterostructures were painted on a highly doped silicon substrate covered with a Au layer of 300 nm thick for FE measurements.[35] Figure 7 shows typical current density-electric field characteristics. The turn-on field ($E_{to}$) and the threshold field ($E_{thr}$) are defined as the electric fields required to produce a current density of 10 $\mu A\ cm^{-2}$ and 10 $mA\ cm^{-2}$, respectively. The $E_{to}$ and $E_{thr}$ of the ZnS tetrapod tree-like heterostructures were 2.66 V $\mu m^{-1}$ and 4.01 V $\mu m^{-1}$, as shown in Figure 7a. The $E_{to}$ is lower than that of the reported ZnS nanobelts (3.47,[36] 3.55,[37] 3.8,[38] V $\mu m^{-1}$) at the similar gap between the anode and the cathode. The current density was about 33.5 $mA\ cm^{-2}$ at a macroscopic field of 4.33 V $\mu m^{-1}$, which is far larger than the reported 14.6 $mA\ cm^{-2}$ or 11.5 $mA\ cm^{-2}$.[39] The superior FE performance suggest that the present ZnS tetrapod tree-like heterostructures can be good field emitters which rival previously reported ZnO,[40] ZnS,[36–38,41,42] Si,[43] SiC,[44] $TiO_2$,[45] AlN,[46] and carbon nanotubes.[47] The reason for the low $E_{to}$ and large stable current density can be probably attributed to the following factors: (1) the high crystalline

structure and cone-shape patterned emission branch with nanometer-sized tip; (2) good contact between the substrate and the nanostructures; (3) free of pollution, (4) the absence of catalysts or additives and (5) the chemical stability and structural rigidity of ZnS nanostructures with high purity.

The FE current-voltage characteristics were analyzed by the Fowler–Nordheim (FN) equations:

$$J = (A\beta^2E^2/\Phi)\exp[-B\Phi^{3/2}(\beta E)^{-1}] \quad (1)$$

$$\text{Or } \ln(J/E^2) = \ln(A\beta^2/\Phi) - B\Phi^{3/2}/\beta E \quad (2)$$

where $J$ is the current density, $E$ is the applied electric field, $\Phi$ is the work function of the emitting materials, which is 7.0 eV for ZnS.[48] $A$ and $B$ are constants with the values of $1.56 \times 10^{-10}$ A eV $V^{-2}$ and $6.83 \times 10^3$ $eV^{-3/2}$ $\mu m^{-1}$. $\beta$ is the field-enhancement factor, which is related to the emitter geometry, crystal structure, and spatial distribution of the emitting centers. Ren et al. demonstrated that the FE performance of ZnO nanowires/nanobelts can be significantly enhanced by increasing the field-enhancement factor via either changing the geometry configuration, decreasing the area density of the nanowires, or increasing the nanowire/nanobelt aspect ratio.[49] ZnS tetrapod tree-like heterostructures have the pattern branch with a cone-shaped geometry configuration and high aspect ratio nanotip. Therefore it is reasonable that they possess high field-enhancement factor. Figure 7b shows the slope of $\ln(J/E^2)$–$(1/E)$ plots. The plot has an approximately linear relation within the measurement range, which confirms that such novel structure can be used as optimal field emitters. The field enhancement factor $\beta$ can be calculated from the slope of the FN plot if the work function of the emitter is known. Based on the reported value of work function of ZnS (7.0 eV), the estimated $\beta$ value is as high as 2600, which is sufficient for various field emission applications. The larger $\beta$ value than those of the reported ZnS[39] should be attributed to the geometrical features (nanosized cone-shape and patterned tips) and single crystallinity. Figure 7c shows variations of emission current density of ZnS tetrapod tree-like heterostructures within 700 minutes at an applied electric field of 4.01 V $\mu m^{-1}$. The initial current density and the average current density are 9.99 mA $cm^{-2}$ and 10.09 mA $cm^{-2}$. No notable current density degradation was observed, and the emission current fluctuation was as low as ~1%, proving the high stability of the ZnS emitter. In fact, the defects in tetrapod ZnS crystalline nanostructures could make electron migration more serious at high electronic fields. From above CL spectra analysis, ZnS tetrapod tree-like heterostructures only show strong emission in the ultraviolet (UV) region. The absence of a broad visible region, which usually is due to radiative recombination of generated holes with electrons occupying the ionized vacancy, confirmed high-quality ZnS nanostructures free of defects, which facilitates stabilizing the emission current. Moreover, a given FE device exhibits poor stability if the emitter is not thermally stable, because much heat is generated when a high electric field is applied to it. The stable FE performance shown in this work is related to ZnS tetrapod tree-like heterostructures with four patterned branches, which have a large contact area that can quickly transfer the heat from the tip to the substrate, so the cone-shape tip can be effectively protected from being destroyed due to superheat.

## 3. Conclusions

We demonstrated that the polarity of the ZnS (111)/(0001) surfaces plays an important role in determining the novel ZnS tetrapod tree-like tetrapod heterostructures. Such a structure is uniquely composed of two phases: a ZB core and hexagonal WZ branches. Through comprehensive HRTEM studies, it is clear that Zn-terminated ZnS (111)/(0001) polar surface is chemically active, inducing the growth of the ZnS wurtzite branches, and the sulfur terminated $(\bar{1}\bar{1}\bar{1})/(000\bar{1})$ polar surface is inert toward the growth of the branched structures. Two strong UV emissions centered at 3.68 and 3.83 eV were observed and attributed to bandgap emissions from the ZB trunk and hexagonal WZ branch, indicating that such structures can be used as unique electromechanical and optoelectronic components in potential light sources, laser and light emitting display devices and medical diagnostics. FE measurements show a low turn-on field of 2.66 V $\mu m^{-1}$, a high field-enhancement factor (over 2600), large current density (over 30 mA $cm^{-2}$ at a macroscopic field of 4.33 V $\mu m^{-1}$) and lower fluctuation of FE current as small as 1%, which is comparable or even better than those of many other nanomaterials. This excellent field-emission property is attributed to the specific crystallographic feature with high crystallinity and cone-shape patterned branch with nanometer-sized tips. Such a structure can optimize the FE properties and make a promising field emitter

## 4. Experimental

*Synthesis of ZnS Nanostructures*: ZnS nanostructures were synthesized, in a horizontal multiple-zone tube furnace, by thermal evaporation of commercially available ZnS powders (< 1 μm in size) at a temperature of 1200 °C and a pressure of 1500 Pa maintained by a $NH_3$ flux at ca. 80 sccm (standard cubic centimeter per minute). No catalysts were used in the experiment. The evaporation was carried out for 2 hrs at the peak temperature. During evaporation, the product was deposited onto a quartz plate that was placed at the downstream end of the furnace with the deposition temperature of ca. 750 °C.

*Structural Characterization*: The synthesized products were characterized using high-resolution X-ray diffraction INT2200, Cu Kα), scanning electron microscopy (SEM JEOL 890 and JEOL 6400), and transmission electron microscopy (TEM) [FEI Tecnai F30 equipped with electron energy loss spectroscopy (EELS) and FEI Tecnai F20 equipped with energy-dispersive X-ray spectroscopy (EDS)].

*Cathodoluminscence (CL) Characterization*: Spatially resolved CL measurements and *in situ* CL imaging of dual phase ZnS tetrapod tree-like heterostructures were carried out (TFE-SEM, Hitachi S4200). The samples were first deposited on a standard copper TEM grid and thoroughly characterized using TEM, and were then used for CL

ADVANCED FUNCTIONAL MATERIALS



characterization. CL spectra of dual phase ZnS tetrapod tree-like heterostructures were collected at the room temperature using a high-resolution CL system operating at an accelerating voltage of 5 kV and a current of 1.2 nA.

*Field Emission*: The field emission property of dual phase ZnS tetrapod tree-like heterostructures was measured in a ball-type chamber which was pumped down to $5 \times 10^{-7}$ Pa by an ultrahigh vacuum system. The anode was a cylinder-shaped platinum probe with 1 mm diameter and dual phase ZnS tetrapod tree-like heterostructures painted on a highly doped silicon substrate covered with a Au layer of 300 nm thick was fixed onto a copper stage as the cathode. The distance between them is 200 μm. High voltage was supplied by a power source (Keithley 248) and the according current signal under increasing applied field in the range of 200 V to 1200 V was recorded by an electrometer (Keithley 6514) with pico-ampere sensitivity.

Received: April 1, 2008
Revised: July 7, 2008
Published online: September 22, 2008

[1] C. Dekker, *Phys. Today* **1999**, *52*, 22.
[2] Z. L. Wang, X. Y. Kong, J. M. Zuo, *Phys. Rev. Lett.* **2003**, *91*, 185502.
[3] A. R. Smith, R. M. Feenstra, D. W. Greve, J. Neugebauer, J. E. Northrup, *Phys. Rev. Lett.* **1997**, *79*, 3934.
[4] X. Fan, X. M. Meng, X. H. Zhang, W. S. Shi, W. J. Zhang, J. A. Zapien, C. S. Lee, S. T. Lee, *Angew. Chem. Int. Ed.* **2006**, *45*, 2568.
[5] Y. F. Hao, G. W. Meng, Z. L. Wang, C. H. Ye, L. D. Zhang, *Nano Lett.* **2006**, *6*, 1650.
[6] X. Y. Kong, Z. L. Wang, *Nano Lett.* **2003**, *3*, 1625.
[7] X. Y. Kong, Y. Ding, R. Yang, Z. L. Wang, *Science* **2004**, *303*, 1348.
[8] D. Moore, Y. Ding, Z. L. Wang, *Angew. Chem. Int. Ed.* **2006**, *45*, 5150.
[9] W. L. Hughes, Z. L. Wang, *J. Am. Chem. Soc.* **2004**, *126*, 6703.
[10] K. A. Dick, K. Deppert, M. W. Larsson, T. Martensson, W. Seifert, L. R. Wallenberg, L. Samuelson, *Nat. Mater.* **2004**, *3*, 380.
[11] L. Manna, D. J. Milliron, A. Meisel, E. C. Scher, A. P. Alivisatos, *Nat. Mater.* **2003**, *2*, 382.
[12] Y. C. Zhu, Y. Bando, D. F. Xue, D. Golberg, *J. Am. Chem. Soc.* **2003**, *125*, 16196.
[13] D. V. Talapin, J. H. Nelson, E. V. Shevchenko, S. Aloni, B. Sadtler, A. P. Alivisatos, *Nano Lett.* **2007**, *7*, 2951.
[14] P. Peng, D. J. Milliron, S. M. Hughes, J. C. Johnson, A. P. Alivisatos, R. J. Saykally, *Nano Lett.* **2005**, *5*, 2651.
[15] Z. G. Chen, A. Ni, F. Li, H. T. Cong, H. M. Cheng, G. Q. Lu, *Chem. Phys. Lett.* **2007**, *434*, 301.
[16] J. F. Gong, S. G. Yang, H. B. Huang, J. Duan, H. W. Liu, X. N. Zhao, R. Zhang, Y. W. Du, *Small* **2006**, *2*, 732.
[17] Z. Q. Deng, J. J. Qi, Y. Zhang, Q. L. Liao, Y. H. Huang, *Nanotechnology* **2007**, *18*, 475603.
[18] G. Z. Shen, Y. Bando, J. Q. Hu, D. Golberg, *Appl. Phys. Lett.* **2007**, *90*, 123101.
[19] Y. C. Zhu, Y. Bando, L. W. Yin, *Adv. Mater.* **2004**, *16*, 331.
[20] V. K. Lazarov, J. Zimmerman, S. H. Cheung, L. Li, M. Weinert, M. Gajdardziska-Josifovska, *Phys. Rev. Lett.* **2005**, *94*, 216101.
[21] S. Lavagne, C. Roucau, C. Levade, G. Vanderschaeve, *Philos. Mag. A* **2002**, *82*, 1451.
[22] Y. Ding, Z. L. Wang, T. J. Sun, J. S. Qiu, *Appl. Phys. Lett.* **2007**, *90*, 153510.
[23] Y. Ding, X. Y. Kong, Z. L. Wang, *J. Appl. Phys.* **2004**, *95*, 306.
[24] C. Y. Yeh, Z. W. Lu, S. Froyen, A. Zunger, *Phys. Rev. B* **1992**, *46*, 10086.
[25] H. Groiss, W. Heiss, F. Schaffler, R. Leitsmann, F. Bechstedt, K. Koike, H. Harada, M. Yano, *J. Cryst. Growth* **2007**, *301*, 671.
[26] J. Y. Lao, J. G. Wen, Z. F. Ren, *Nano Lett.* **2002**, *2*, 1287.
[27] T. K. Tran, W. Park, W. Tong, M. M. Kyi, B. K. Wagner, C. J. Summers, *J. Appl. Phys.* **1977**, 2803.
[28] H. C. Ong, R. P. H. Chang, *Appl. Phys. Lett.* **2001**, *79*, 3612.
[29] E. Schlam, *Proc. IEEE* **1973**, *61*, 894.
[30] G. Schlegel, J. Bohnenberger, I. Potapova, A. Mews, *Phys. Rev. Lett.* **2002**, *88*, 137401.
[31] M. Cardona, G. Harbeke, *Phys. Rev.* **1965**, *137*, A1467.
[32] O. Zakharov, A. Rubio, X. Blase, M. L. Cohen, S. G. Louie, *Phys. Rev. B* **1994**, *50*, 10780.
[33] B. W. Jacobs, V. M. Ayres, M. P. Petkov, J. B. Halpern, M. Q. He, A. D. Baczewski, K. McElroy, M. A. Crimp, J. M. Zhang, H. C. Shaw, *Nano Lett.* **2007**, *7*, 1435.
[34] J. H. Yu, J. Joo, H. M. Park, S. I. Baik, Y. W. Kim, S. C. Kim, T. Hyeon, *J. Am. Chem. Soc.* **2005**, *127*, 5662.
[35] Q. H. Li, Q. Wan, Y. J. Chen, T. H. Wang, H. B. Jia, D. P. Yu, *Appl. Phys. Lett.* **2004**, *85*, 636.
[36] X. S. Fang, Y. Bando, G. Z. Shen, C. H. Ye, U. K. Gautam, P. M. F. J. Costa, C. Y. Zhi, C. C. Tang, D. Golberg, *Adv. Mater.* **2007**, *19*, 2593.
[37] X. S. Fang, Y. Bando, C. H. Ye, D. Golberg, *Chem. Commun.* **2007**, 3048.
[38] F. Lu, W. P. Cai, Y. G. Zhang, Y. Li, F. Q. Sun, S. H. Heo, S. O. Cho, *Appl. Phys. Lett.* **2006**, *89*, 23 1928.
[39] X. Fang, Y. Bando, U. K. Gautam, C. Ye, D. Golberg, *J. Mater. Chem.* **2008**, *18*, 509.
[40] C. J. Lee, T. J. Lee, S. C. Lyu, Y. Zhang, H. Ruh, H. J. Lee, *Appl. Phys. Lett.* **2002**, *81*, 3648.
[41] Y. Q. Chang, M. W. Wang, X. H. Chen, S. L. Ni, W. J. Qiang, *Solid State Commun.* **2007**, *142*, 295.
[42] P. K. Ghosh, U. N. Maiti, S. Jana, K. K. Chattopadhyay, *Appl. Surf. Sci.* **2006**, *253*, 1544.
[43] N. G. Shang, F. Y. Meng, F. C. K. Au, Q. Li, C. S. Lee, I. Bello, S. T. Lee, *Adv. Mater.* **2002**, *14*, 1308.
[44] Z. W. Pan, H. L. Lai, F. C. K. Au, X. F. Duan, W. Y. Zhou, W. S. Shi, N. Wang, C. S. Lee, N. B. Wong, S. T. Lee, S. S. Xie, *Adv. Mater.* **2000**, *12*, 1186.
[45] J. M. Wu, H. C. Shih, W. T. Wu, *Chem. Phys. Lett.* **2005**, *413*, 490.
[46] Y. B. Tang, H. T. Cong, Z. G. Chen, H. M. Cheng, *Appl. Phys. Lett.* **2005**, *86*, 233104.
[47] W. A. Deheer, A. Chatelain, D. Ugarte, *Science* **1995**, *270*, 1179.
[48] L. J. V. Ruyven, F. E. Williams, *Phys. Rev. Lett.* **1966**, *16*, 889.
[49] W. Z. Wang, B. Q. Zeng, J. Yang, B. Poudel, J. Y. Huang, M. J. Naughton, Z. F. Ren, *Adv. Mater.* **2006**, *18*, 3275.